IEEE Open Journal of
Industry Applications

Received 16 March 2022; revised 9 May 2022 and 17 June 2022; accepted 27 June 2022. Date of publication 14 July 2022;
date of current version 25 July 2022. The review of this article was arranged by Associate Editor Mauro Di Nardo.

Digital Object Identifier 10.1109/OJIA.2022.3190905

Torque Ripple Minimization Control Strategy in Synchronous Reluctance Machines

ANANT K SINGH [1,2] (Member, IEEE), RAMAKRISHNAN RAJA [1] (Senior Member, IEEE), TOMY SEBASTIAN [1] (Fellow, IEEE), AND KAUSHIK RAJASHEKARA [2] (Life Fellow, IEEE)

[1]Halla Mechatronics, Bay City, MI 48706 USA
[2]University of Houston, Houston, TX 77004 USA

CORRESPONDING AUTHOR: ANANT K SINGH (e-mail: anant.singh@halla.com)

ABSTRACT Torque smoothness is an essential requirement for high-performance motor drive applications. Synchronous reluctance machines (SyRM) have high torque ripple due to non-linear magnetic circuit and saturation. Typically, in Permanent magnet machines the active torque ripple compensation is achieved by injecting a compensating ripple current in the *q-axis*. For SyRM, the current injection method for active torque ripple cancellation can be used in both the *d-axis* and *q-axis*. However, the saturation of the motor parameters with the changing current can result in varied performance between the two methods. This paper evaluates the effectiveness of both of these methods for torque ripple cancellation. For evaluation, the impact of parameter saturation with ripple current injection on the *d-axis* and the *q-axis* is studied. The mathematical conclusions obtained are evaluated by both the simulation and the experimental results performed on a 4 pole 1200W Synchronous reluctance machine.

INDEX TERMS Active torque ripple compensation, motor control, synchronous reluctance machine, torque ripple.

I. INTRODUCTION

The synchronous reluctance machines (SyRM) are proving to be potential alternatives to permanent magnet machines. They are currently limited to non-high performance motor drive applications in most cases due to their high torqxue ripple. There are several methods studied in the literature to optimize the torque ripple in SyRM. These methods can be categorized into machine design and control methods. The machine design approach involves optimizing the machine structure such as the flux barriers, rotor rib, and rotor skewing. Different design refinement methods utilizing FEA are studied in [1], [2]. In [3]–[7], the influence of the different rotor geometries is investigated to optimize both the average torque and the torque ripple. A hybrid permanent magnet synchronous reluctance machine with axially sandwiched magnets is studied in [2], for improving the overall machine performance which includes the average torque and the torque ripple. A combination of asymmetrical barriers along with the hybrid magnetic core for the torque ripple reduction method is investigated in [8].

In control based approaches, the basic idea is to add selected current harmonics to the original stator currents to reduce the torque ripple. In [9], the optimal currents for compensating the torque harmonics are obtained using a torque function. This torque function is obtained by injecting the sinusoidal stator current to the finite element model of the SyRM and profiling the obtained torque output. In [10], direct torque control method is investigated for the torque ripple reduction. The direct torque is combined with flux control in [11]. The advantage of active cancellation methodology compared to machine design optimization is that the machine design can be relaxed and manufacturing of such drives becomes easier.

In this paper, the control approach of active torque ripple cancellation for minimizing the torque ripple is investigated. The active torque ripple cancellation method actively controls the excitation current waveforms to generate a smooth output torque. The term "active" in this paper means a methodology to cancel machine torque ripple while the machine is operating at various torque-speed conditions. The active torque ripple cancellation has been used in the industry for decades and is a norm in most high-performance electric drive applications. Most of the available literature does active torque ripple

cancellation using current injection [9]–[23]. Some other literature suggests voltage injection methods for torque ripple cancellation [24], [25]. However, the voltage based cancellation techniques are not very effective as the performance of these methods is highly dependent on the motor parameter and accurate measurement of speed. When employing the current injection method for torque ripple cancellation, it is also important to consider the saturation of the machine. A higher magnitude of current will cause more saturation in the machine. Therefore, optimizing the magnitude of the injected cancellation current becomes a critical factor when using current based methods for active torque ripple cancellation.

The objective of this paper is to evaluate the difference between the *d-axis* and *q-axis* current injection methods for torque ripple cancellation in Synchronous Reluctance machines. The current injection based methods in the present literature [9]–[12] don't distinctively identify whether the *d-axis* or the *q-axis* current injection is better for torque ripple cancellation. The machine saturation acts differently with *d* and *q-axis* current injection at different operating conditions for Synchronous reluctance machines, which is the focus of investigation in this paper. In Section II of the paper, the effect of the parameter saturation on the active torque ripple compensation using current injection is studied. In this section *d* and *q-axis* current based methods are compared to evaluate the magnitude of torque developed per ampere of injected cancellation current. The simulation results are presented in Section III. The control strategy employed for implementing the active cancellation approach is discussed in Section IV. The simulation results are validated through experimental results obtained using a 1200W 30 Slot 4 pole pure SyRM machine, in Section V. The paper is concluded with a strategy to calculate the best compensation method based on the operating condition of the motor especially when the motor parameter saturation becomes significant as in the case of pure SyRM.

II. EFFECT OF PARAMETER SATURATION ON THE ACTIVE TORQUE RIPPLE COMPENSATION

In the active torque ripple cancellation method, the torque ripple is measured and a ripple current component is calculated that can effectively cancel the torque ripple produced by the machine by applying a torque opposite to the machine's torque ripple component. Fig. 1 shows the experimental comparison between the uncompensated and compensated torque ripple for a 8 pole 12 slot IPM machine using the active torque ripple compensation method. The torque ripple compensation component was applied in the *q-axis* current for obtaining the results in Fig. 1.

In Interior Permanent Magnet (IPM) machine the torque developed by the machine is the sum of torque generated by the back emf (BEMF) portion and the reluctance portion. The torque equation for an IPM machine is:

$$T = \frac{3}{2}K_e I_q + \frac{3P}{4}\left(L_{qsat} - L_{dsat}\right) I_q I_d \qquad (1)$$

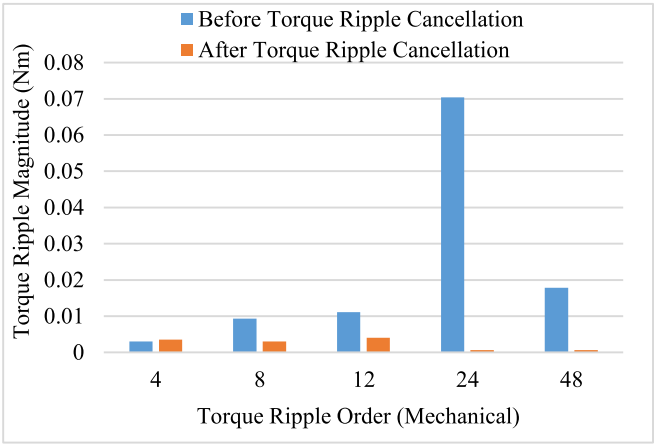

FIGURE 1. Experimental comparison between uncompensated and compensated torque ripple measured at 40RPM in an 8 pole 12 slot IPM machine at peak torque output of 5Nm, using compensation current in q-axis.

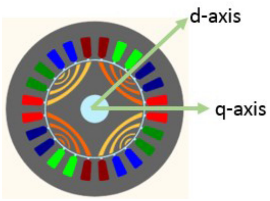

FIGURE 2. Definition of *q* and *d-axis*.

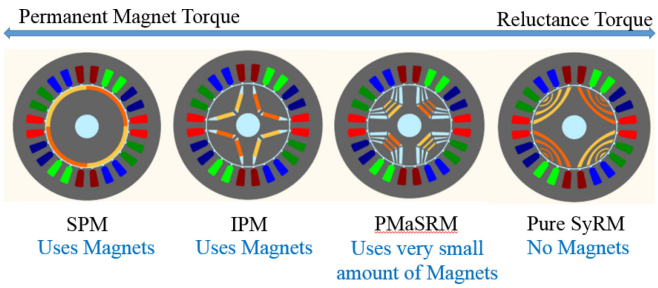

FIGURE 3. Contribution of reluctance torque and permanent magnet torque in different machine types.

Where T is the electromagnetic torque developed by the machine, K_e is the BEMF constant of the machine, I_q and I_d are the quadrature and direct axis currents, L_{qsat} and L_{dsat} are the saturated quadrature and direct axis inductances and P is the number of poles of the machine. The definition of the *q* and *d-axis* is shown in Fig. 2.

In general, the current cancellation component for active torque ripple cancellation is applied on the quadrature axis. The reason for applying the current cancellation component on the quadrature axis is the fact that most of the torque generated in the case of a permanent magnet machine is contributed by the magnet portion.

Fig. 3 shows the qualitative comparison of the torque contribution between the permanent magnet and the reluctance portion in different machine types. The majority of the torque in the case of IPM machines is generated from the BEMF

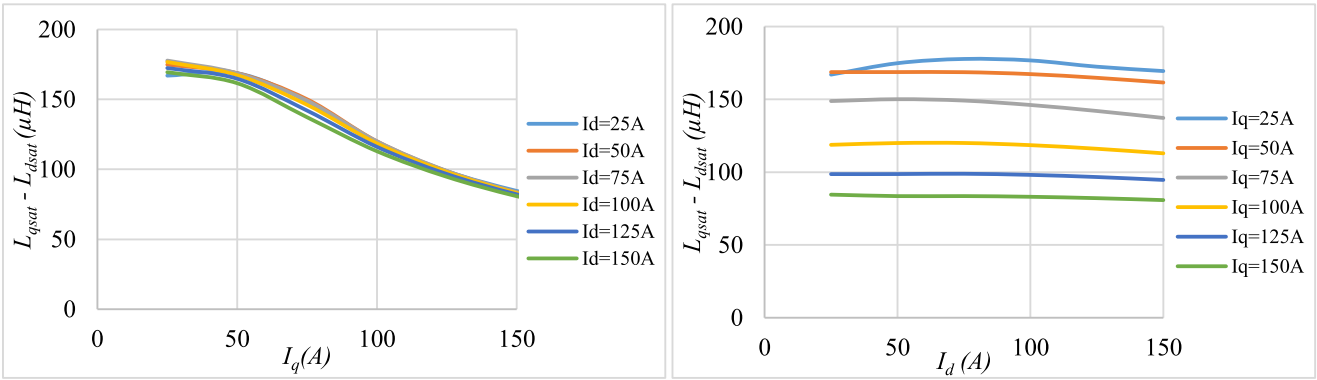

FIGURE 4. $L_{qsat} - L_{dsat}$ saturation for pure SyRM machine of Table 1 as a function of I_q and I_d.

portion of the machine. In the case of the Surface Permanent Magnet (SPM) machine where L_d is approximately equal to L_q, there is no reluctance portion of the torque. Thus for SPM machines using quadrature axis current for compensating torque ripple is the obvious choice.

The torque developed by the machine when cancellation current is injected in the *q-axis* can be written as:

$$T = \frac{3}{2}K_e\left(I_{q0} + i_{qr,n}\right) + \frac{3P}{4}\left(L_{qsat} - L_{dsat}\right)\left(I_{q0} + i_{qr,\,n}\right)I_{d0} \tag{2}$$

Where I_{q0} and I_{d0} are the dc components of q and *d-axis* currents and the $i_{qr,n}$ is the instantaneous injected cancellation component of n^{th} order. $i_{qr,n}$ is represented as:

$$i_{qr,n} = I_{qr,n}\sin\left(n\theta + \emptyset_{r,n}\right) \tag{3}$$

Where $I_{qr,n}$ and $\emptyset_{r,n}$ are the magnitude and the phase of the injected ripple component, θ is the mechanical motor position and n is the torque ripple order which needs to be compensated. The $I_{qr,n}$ and the $\emptyset_{r,n}$ values change as a function of current such that it negates the torque ripple developed by the machine.

In the case of IPM machines, if the cancellation current is applied in the *d-axis*, only the reluctance component of torque would contribute to the active torque ripple cancellation. Therefore the magnitude of the injected cancellation current would be much larger.

In another possible scenario, if the cancellation current is applied in both *d* and *q-axis* currents at the same time then in addition to the intended torque ripple orders, some undesired orders of torque ripple will be created. This is because of the interaction of different sinusoidal components at the same instant.

In the case of pure SyRM, no torque is generated from the BEMF portion of the machine. The only torque produced by the machine is the reluctance torque. Thus the torque equation of the SyRM can be rewritten from (1) as:

$$T = \frac{3P}{4}\left(L_{qsat} - L_{dsat}\right)I_qI_d \tag{4}$$

In the case of SyRM, from (4) it can be perceived that injecting the ripple component in either *q-axis* or *d-axis* current should be possible. The main goal is to thus identify which method between the two can provide larger torque for a given magnitude of cancellation current. By differentiating (4) with respect to I_d and I_q, it can be established which of the two methods will provide more torque for a given current. Differentiating (4) with respect to I_q and I_d can be expressed as:

$$\frac{dT}{dI_q} = I_d\left(\frac{3P}{4}\left(L_{qsat} - L_{dsat}\right)\right) + \frac{3P}{4}\left(\frac{dL_{qsat}}{dI_q} - \frac{dL_{dsat}}{dI_q}\right)I_qI_d \tag{5}$$

$$\frac{dT}{dI_d} = I_q\left(\frac{3P}{4}\left(L_{qsat} - L_{dsat}\right)\right) + \frac{3P}{4}\left(\frac{dL_{qsat}}{dI_d} - \frac{dL_{dsat}}{dI_d}\right)I_qI_d \tag{6}$$

Fig. 4 shows the $(L_{qsat} - L_{dsat})$ as a function of I_q and I_d currents. Using this information in (5) and (6) the $\frac{dT}{dI_q}$ and $\frac{dT}{dI_d}$ can be evaluated. If $\frac{dT}{dI_q}$ is greater than $\frac{dT}{dI_d}$, it can be concluded that the compensation using *q-axis* current injection would be better. This is because the magnitude of the injection current required will be smaller. Similarly if $\frac{dT}{dI_d}$ is greater then it is better to use I_d current injection. Fig. 4 includes the effect of L_q and L_d saturation due to both I_q and I_d. This also includes the cross-coupling effects.

For the SyRM parameters shown in Table 1, $\frac{dT}{dI_q}$ and $\frac{dT}{dI_d}$ are evaluated. When these parameters are equal, either of the *q-axis* or the *d-axis* based current injection method will perform the same. Fig. 5 shows a boundary line on the *d*- and *q*-axis current graph where one method is better than the other. Depending on the operating point (I_q, I_d), cancellation current injection in the *d-axis* or *q-axis* can be selected.

Further by calculating the ratio of $\frac{dT}{dI_q}$ and $\frac{dT}{dI_d}$, the magnitude difference between the two methods can be quantified. This calculation is performed on the motor parameters obtained from the FEA results. Fig. 6 shows the theoretical

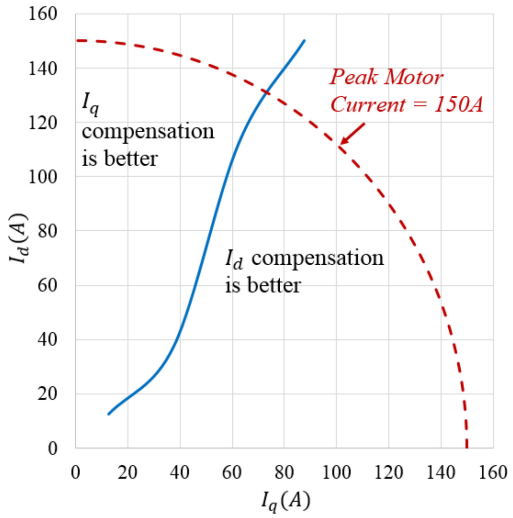

FIGURE 5. Boundary line separating the dq current combinations where d or q-axis based compensation is better, for machine parameters shown in Table 1.

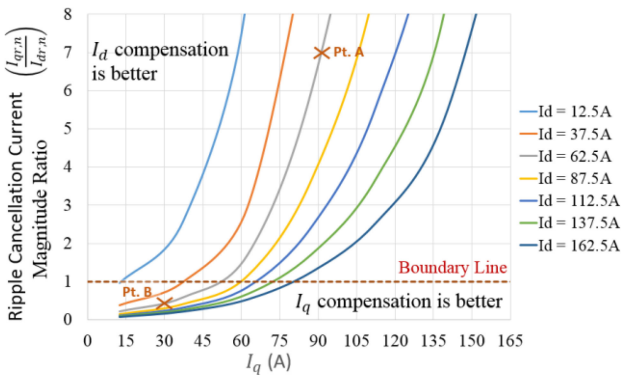

FIGURE 6. Ripple current magnitude comparison between the d and q-axis based current compensation.

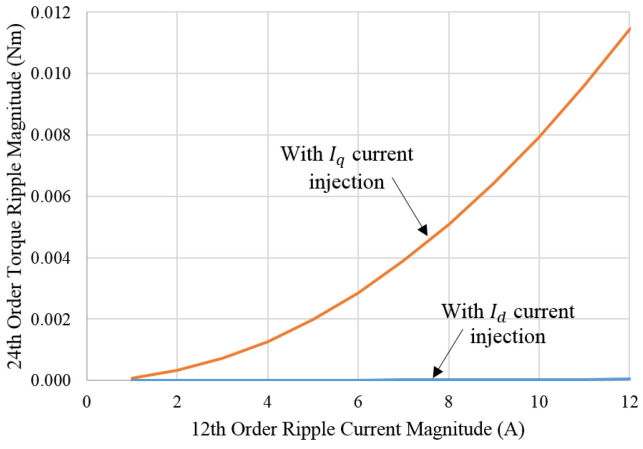

FIGURE 7. 24th order (Undesired) torque ripple magnitude as a function of the injected magnitude of 12th order ripple current in q-axis and d-axis, for Op. 2.

TABLE 1. Machine Parameter for the SyRM Used for Simulation and Experiment Results

$No.of\ slots$	30
$No.of\ poles$	4
L_q	$260\mu H$
L_d	$65\mu H$
R_{ph}	12mΩ
Max motor current	150A
Max Speed	4000 RPM
Peak Power	1200 W
Peak Torque	4 Nm

ratio of compensating current in I_q to that in I_d for the same magnitude of torque ripple $\left(\frac{I_{qr,n}}{I_{dr,n}}\right)$.

As an example, a current combination (Pt. A in Fig. 6) is taken where the *d-axis* current is 62.5A and *q-axis* current is 90A. For this current combination, based on Fig. 6, if a particular order of torque ripple needs 1A with I_d based compensation, it may require ∼7A of ripple current with I_q based compensation.

For another current combination (Pt. B in Fig. 6) chosen below the boundary line where I_q based compensation is better, similar difference in the magnitudes between the two methods can be observed. For Pt. B, the *d-axis* current is 62.5A and *q-axis* current is 30A. For this point, the magnitude of the *q-axis* injection current will be ∼2 times compared to *d-axis*. It is to be noted that these calculations are performed for the machine parameter shown in Table 1. Thus for the example machine at a given operating point, the magnitude of the I_q, I_d combination will determine if I_q ripple injection or I_d ripple injection is better.

In practical applications, there may be several torque ripple orders that are intended to be canceled. Therefore there will be different cancellation current harmonic components that would be injected to get the desired torque ripple performance. To understand the influence of these cancellation current injections on the final output torque ripple, an example case is taken where torque ripple orders of n_1 and $n_2$are desired to be canceled. In this example, cancellation current injection in the *d-axis* is assumed. For canceling the two intended orders, cancellation currents of order n_1 and n_2 are injected into the machine. The torque equation with these cancellation current injections can be written as:

$$T = \frac{3P}{4}\left(L_{qsat} - L_{dsat}\right) I_{q0}\left(I_{d0} + I_{dr,\,n_1}\sin\left(n_1\theta + \emptyset_{n_1}\right) + I_{dr,\,n_2}\sin\left(n_2\theta + \emptyset_{n_2}\right)\right) \quad (7)$$

Where n_1 and n_2 are the orders that are intended to be canceled, $I_{dr,\,n_1}$ and I_{dr,n_2} are the injected current ripple magnitudes, $\emptyset_{n_1}$ and $\emptyset_{n_2}$ are the respective phases.

If the saturation in the motor parameters is small with the cancellation current injection, then the difference between the *q-axis* and *d-axis* inductance$(L_{qsat} - L_{dsat})$ can be considered constant. In this scenario, from (7) the final torque output would contain only the orders of n_1 and n_2.

As the saturation of the machine parameters with the changing current increases or if the magnitude of the injected cancellation current increases then the $(L_{qsat} - L_{dsat})$ difference may not be considered constant. To best represent the $(L_{qsat} - L_{dsat})$ difference as a function of changing current, it is linearized around an operating point. With this representation, the $(L_{qsat} - L_{dsat})$ difference will vary sinusoidally following the shape of the sinusoidal injected ripple component. This is because the saturation value at every point of the injected ripple current will be different. Thus the $(L_{qsat} - L_{dsat})$ difference can be approximated as:

$$\left(L_{qsat} - L_{dsat}\right) = L_{qd0} - \sum_{k=1}^{r} L_{qd_k} I_{r,k} sin\left(k\theta + \emptyset_k\right) \quad (8)$$

Where L_{qd0} is the dc component of the difference, L_{qd_k} is the slope of the $(L_{qsat} - L_{dsat})$ term around an operating point at which the compensating current is injected, $I_{r,k}$ is the magnitude of the injected compensating current and $\emptyset_k$ is the phase of the k^{th} order of injected compensating current and r is the general representation of any order. It is to be noted that the sign of the L_{qdk} term is always going to be opposite to the injected ripple current $(I_{dr,n}\ or\ I_{qr,n})$ component. This is because the saturation increases with the increasing current thereby reducing the $(L_{qsat} - L_{dsat})$ difference and vice versa. In this example, k has only two values n_1 and n_2. From (7) and (8) the torque can be written as:

$$\begin{aligned} T = \frac{3P}{4} \Big(& L_{qd0} - L_{qd_{n_1}} I_{dr,n_1} \sin\left(n_1\theta\right) \\ & - L_{qd_{n_2}} I_{dr,n_2} \sin\left(n_2\theta\right) \Big) I_{q0} \left(I_{d0}\right. \\ & \left. + I_{dr,n_1} \sin\left(n_1\theta\right) + I_{dr,n_2} \sin\left(n_2\theta\right) \right) \end{aligned} \quad (9)$$

The value of $\emptyset_k$ is assumed to be zero for simplicity. (9) can be further simplified as shown:

$$\begin{aligned} T = \frac{3PI_{q0}}{4} \Bigg\{ & \left(L_{qd0} I_{d0} - \frac{L_{qd_{n_1}} I_{dr,n_1}^2}{2} - \frac{L_{qd_{n_2}} I_{dr,n_2}^2}{2} \right) \\ & + \left(L_{qd0} I_{dr,n_1} - L_{qd_{n_1}} I_{dr,n_1} I_{d0} \right) \sin\left(n_1\theta\right) + \left(L_{qd0} I_{dr,n_2} \right. \\ & \left. - L_{qd_{n_2}} I_{dr,n_2} I_{d0} \right) \sin\left(n_2\theta\right) - L_{qd_{n_1}} I_{dr,n_1}^2 \cos\left(2n_1\theta\right) \\ & - L_{qd_{n_2}} I_{dr\mathrm{n}_2}^2 \cos\left(2n_2\theta\right) \\ & - \frac{I_{dr,\mathrm{n}_1} I_{dr,\mathrm{n}_2} \left(L_{qd_{n_1}} + L_{qd_{n_2}} \right) \cos\left(n_1 - n_2\right)\theta}{2} \\ & + \frac{I_{dr,\mathrm{n}_1} I_{dr,\mathrm{n}_2} \left(L_{qd_{n_1}} + L_{qd_{n_2}} \right) \cos\left(n_1 + n_2\right)\theta}{2} \Bigg\} \end{aligned} \quad (10)$$

It can be observed from (10) that the injection of current components of orders n_1 and n_2 created desired torque ripple of orders n_1 and n_2 but also undesired torque ripple of orders $2n_1,\ 2n_2,\ (n_1 + n_2)\ and\ (n_1 - n_2)$. In addition to the injected current magnitudes, the magnitude of the undesired torque ripple orders is also going to be dependent on the magnitude of L_{qdn_1} and L_{qdn_2} which is a function of the saturation. If the saturation with the cancellation current is small, the magnitude of unintended components of torque ripple becomes negligible. In addition to the undesired ripple components, the saturation also creates a dc component of the torque. The average torque value will decrease as the saturation effect increases. The summary of ripple components is shown in Table 2.

TABLE 2. Summary of Torque Ripple Orders Created With n_1 and n_2 Cancellation Current Injection

Order		*Torque Ripple Magnitude*
DC Component		$\frac{3PI_{q0}}{4}\left(L_{qd0}I_{d0} - \frac{L_{qd_{n_1}}I_{dr,n_1}^2}{2} - \frac{L_{qd_{n_2}}I_{dr,n_2}^2}{2}\right)$
n_1	Desired Orders	$\frac{3PI_{q0}}{4}\left(L_{qd0}I_{dr,n_1} - L_{qd_{n_1}}I_{dr,n_1}I_{d0}\right)$
n_2		$\frac{3PI_{q0}}{4}\left(L_{qd0}I_{dr,n_2} - L_{qd_{n_2}}I_{dr,n_2}I_{d0}\right)$
$2n_1$	Undesired Orders	$\frac{3PI_{q0}}{4}L_{qd_{n_1}}I_{dr,n_1}^2$
$2n_2$		$\frac{3PI_{q0}}{4}L_{qd_{n_2}}I_{dr\mathrm{n}_2}^2$
$(n_1 + n_2)$		$\frac{3PI_{q0}I_{dr,\mathrm{n}_1}I_{dr,\mathrm{n}_2}}{4}\left(L_{qd_{n_1}} + L_{qd_{n_2}}\right)$
$(n_1 - n_2)$		$\frac{3PI_{q0}I_{dr,\mathrm{n}_1}I_{dr,\mathrm{n}_2}}{4}\left(L_{qd_{n_1}} + L_{qd_{n_2}}\right)$

TABLE 3. Operating Points for Simulation

Operating Point 1 (Op.1)	I_q = 12.5A and $I_d = 112.5A$
Operating Point 2 (Op.2)	I_q = 112.5A and $I_d = 62.5A$

III. SIMULATION RESULTS

The two operating points shown in Table 3 are chosen to observe the different torque ripple performance behavior on either side of the boundary line shown in Fig. 6.

For the machine parameters shown in Table 1, the dominant magnitudes of torque ripple are of orders 12^{th} and 60^{th}. Figs. 8(a) and 9(a) show the torque ripple obtained from FEA for the 12^{th} and 60^{th} order. For simulation only these two orders are considered as they are the dominant orders. The simulation is performed in MATLAB, by utilizing an equivalent *d-q* model of the SyRM parameters shown in Table 1. The torque ripple is added to the dc torque obtained at a given operating point. The magnitude and order for the torque ripple injected are obtained using FEA simulation. The active ripple compensation current is added to the *d* or the *q-axis* component of the current fed to the equivalent machine model. The simulation was performed at a fixed 40RPM. The simulation results shown in Figs. 8 and 9 compare the magnitudes of the *d* and *q-axis* cancellation current required to cancel the torque ripple at Op.1 and Op.2. The results for Op.1 are shown in Fig. 8 and the results for Op.2 are shown in Fig. 9.

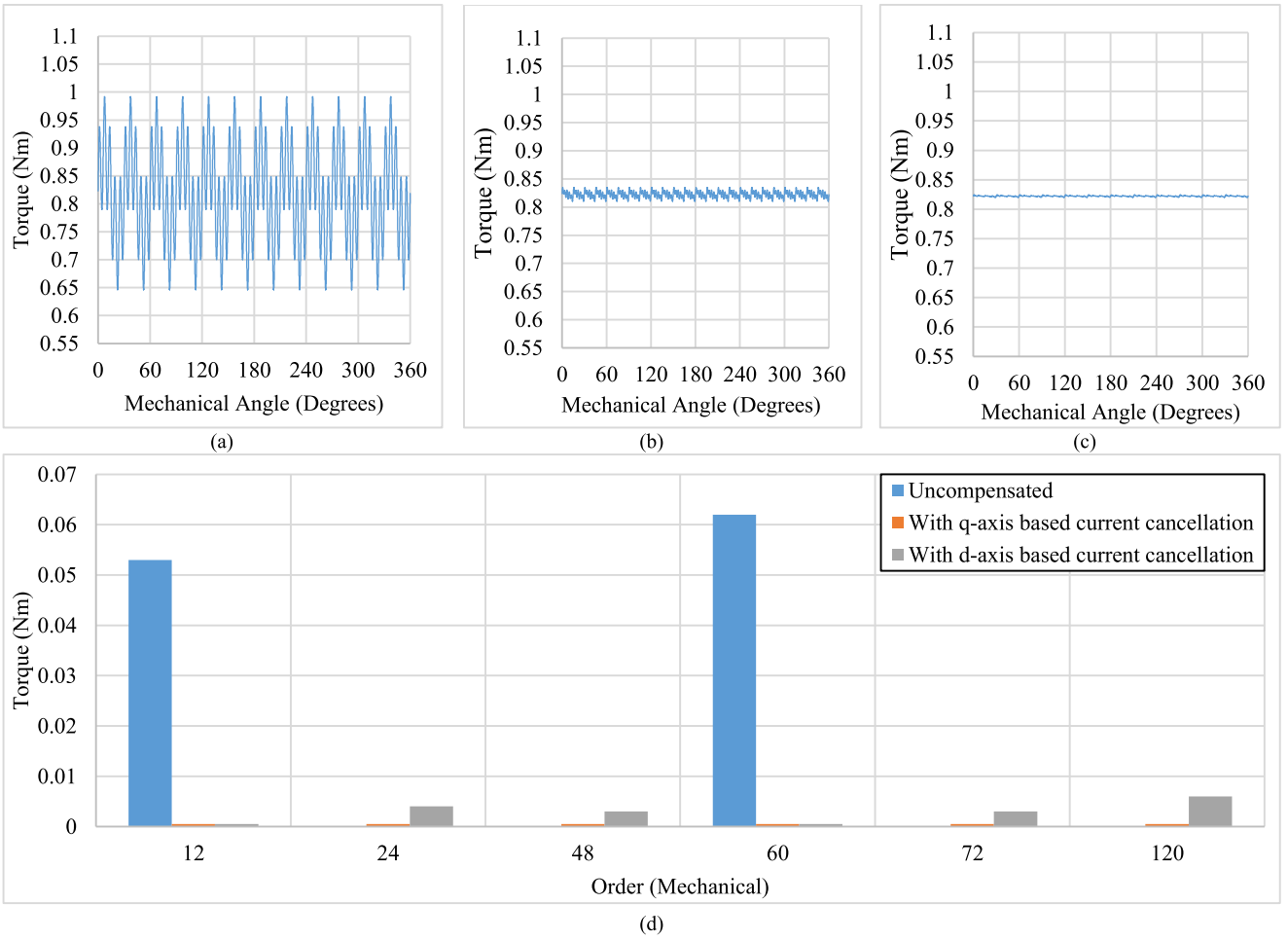

FIGURE 8. Simulation torque ripple results for Op.1 ($I_q = 12.5A$ and $I_d = 112.5A$). (a) Uncompensated torque ripple of the machine. (b) Compensated torque ripple after d-axis current based cancellation with $I_{dr,n_1} = 16.4A$ and $I_{dr,n_2} = 20.1A$. (c) Compensated torque ripple after q-axis current based cancellation with $I_{qr,n_1} = 1.8A$ and $I_{qr,n_2} = 2.1A$. (d) Harmonic component comparison between the uncompensated and compensated torque ripple after d-axis and q-axis current based cancellation.

From Fig. 6, it can be observed that for Op.1, I_q based compensation is better compared to I_d. The calculated I_d injection current magnitude required for canceling the 12^{th} order torque ripple was 16.4A and for the 60^{th} order was 20.1A. While for the I_q based compensation the cancellation current magnitude required was 1.8A for the 12^{th} order and 2.1A for the 60^{th} order. With I_d based compensation, it can be observed that while the 12^{th} and 60^{th} torque ripple orders are canceled but now small magnitudes of undesired 24^{th}, 48^{th}, 72^{nd}, and 120^{th} orders of torque ripple are created which follows (10).

Similarly, for Op.2, it is observed that I_d based compensation is better compared to I_q based compensation. The injection current magnitude required for cancellation with I_d component was 0.8A for the 12^{th} order anvvd 1.3A for the 60^{th} order. While with the I_q component the injection current magnitude was 10.2A for 12^{th} order torque ripple and 16.65A for 60^{th} order. In this case as well, the magnitude of the injected current follows the magnitude ratio shown in Fig. 6. In addition, undesired 24^{th}, 48^{th}, 72^{nd}, and 120^{th} orders of torque ripple are developed, which follows (10). In this case, the undesired component is much higher in magnitude compared to Op.1.

Fig. 7 shows the torque ripple magnitude for the undesired 24^{th} harmonic order as a function of the injected ripple current magnitude of 12^{th} order, for Op. 2. With ripple current injection in the *q-axis*, it can be observed that as the magnitude of ripple current increases, the magnitude of the undesired 24^{th} harmonic order in torque increases. Whereas with ripple current injection in *d-axis,* the magnitude of the undesired 24^{th} order torque ripple is negligible. The observed behavior can be explained by the L_{qdk} term in (8). L_{qdk} is the slope of the $(L_{qsat} - L_{dsat})$ with repsect to I_d for current injection in *d-axis*. From Fig. 4, it can be observed that the slope of the $(L_{qsat} - L_{dsat})$ term with respect to I_d is near zero. Thus the L_{qdk} term becomes negligible with *d-axis* current injection. Thus, it is verified that the magnitude of the undesired torque ripple order is dependent on the magnitude of L_{qdk} which is a function of the saturation due to the injected current magnitude.

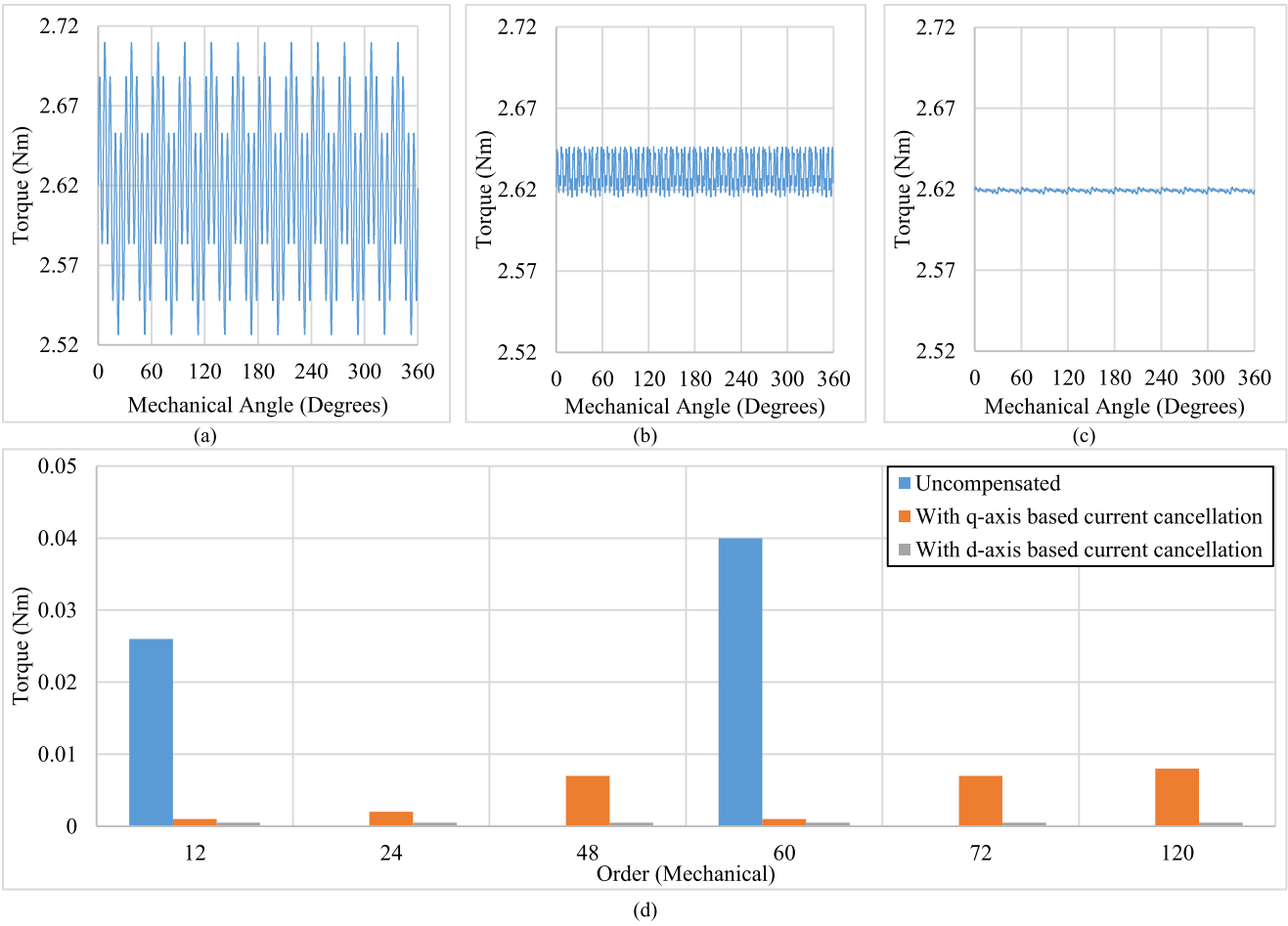

FIGURE 9. Simulation torque ripple results for Op.2 ($I_q = 112.5A$ and $I_d = 62.5A$). (a) Uncompensated torque ripple of the machine. (b) Compensated torque ripple after q-axis current based cancellation with $I_{qr,n_1} = 10.2A$ and $I_{qr,n_2} = 16.65A$. (c) Compensated torque ripple after d-axis current based cancellation with $I_{dr,n_1} = 0.8A$ and $I_{dr,n_2} = 1.3A$. (d) Harmonic component comparison between the uncompensated and compensated torque ripple after q-axis and d-axis current based cancellation.

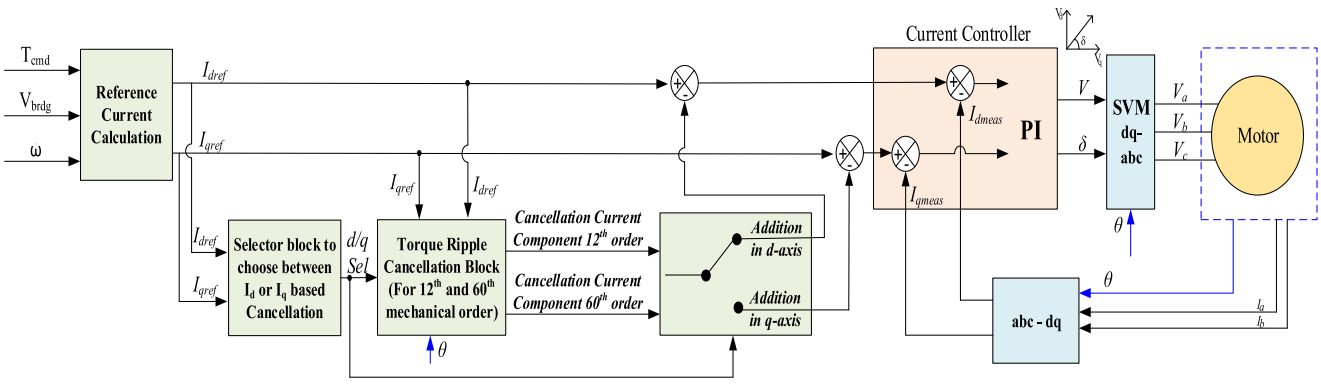

FIGURE 10. Control block diagram for active torque ripple cancellation in SyRM.

IV. CONTROL STRATEGY FOR ACTIVE TORQUE RIPPLE CANCELLATION IN SYNCHRONOUS RELUCTANCE MACHINES

The control strategy for the active torque ripple cancellation is shown in Fig. 10. The control blocks include a reference current generation module, a selector block to choose between *d* or *q-axis* current based cancellation, a torque ripple cancellation block, and a current controller. The reference current calculation module calculates the *d* and *q-axis* reference currents based on the operating inputs. The reference current generation module is covered in detail in [26]. The calculated reference currents are fed to the selector block

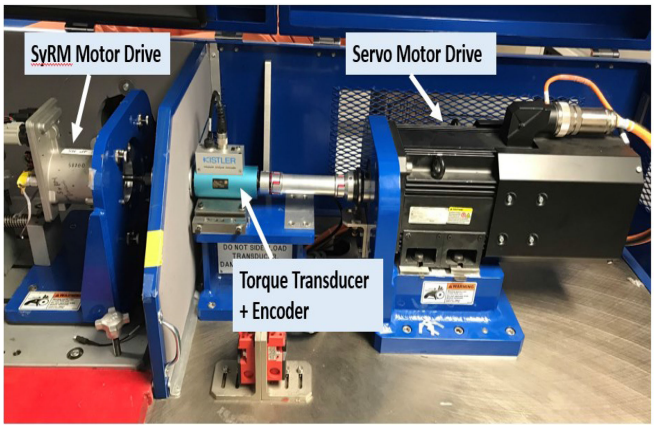

FIGURE 11. Experimental setup.

TABLE 4. Operating Points for Ripple Cancellation Current Magnitude Ratio $\left(\frac{I_{qr.n}}{I_{dr.n}}\right)$ Verification

Operating Points				
I_d *(in A)*	112.5	112.5	112.5	112.5
I_q (in A)	12.5	37.5	62.5	87.5
Summary of ripple cancellation current magnitude ratio from analysis and experiment for 60th order compensation				
Analysis Ratio	0.11	0.32	0.85	2.43
Experimental Ratio	0.11	0.30	0.84	1.99
Experimental *q-axis* based current cancellation magnitude (A)	1.9	1.01	1.56	2.01
Experimental *d-axis* based current cancellation magnitude (A)	17.5	3.31	1.86	1.04

and the torque ripple cancellation block. The selector block chooses between the *d* or *q-axis* based current cancellation as per Fig. 5 created for machine parameters in Table 1. The torque ripple cancellation block then takes the selector block input and calculates the cancellation current magnitude and phase based on a torque ripple calibration table generated offline. The torque ripple orders intended to be canceled are the 12th and 60th order. The cancellation current magnitude and phase are used to modify the reference current fed into the controller.

The current controller implemented has a bandwidth of 1200 Hz. At higher speed, the magnitude and phase of the injected cancellation current is adjusted per the current control frequency response of the system. This concept is covered in [27].

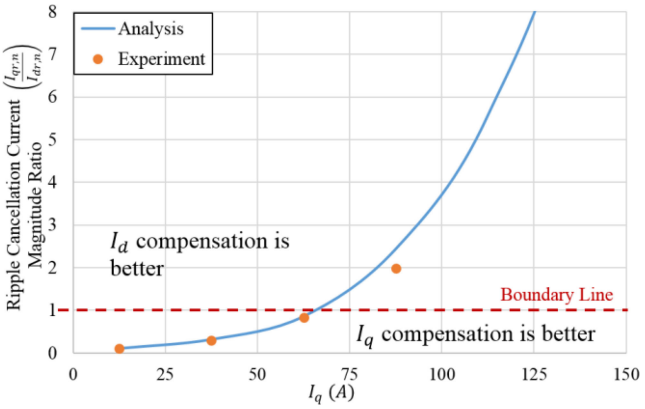

FIGURE 12. Experimental compensation current magnitude comparison between the d and q-axis based current compensation for operating points in Table 4, for 60th order torque ripple cancellation.

V. EXPERIMENTAL RESULTS

In this section, the experimental results for the machine parameters in Table 1 are discussed. For the given machine, the compensation is performed for the 12th and 60th order (mechanical) torque ripple. The primary focus is to study the effectiveness of the *d* or *q-axis* current based cancellation for these two orders. There are other uncompensated torque ripple orders present in the machine which are not considered because of their smaller magnitude. The methodology discussed in the paper can be extended to other torque ripple orders if needed.

The test setup is shown in Fig. 11. The test setup comprises of a servo drive, encoder, torque sensor, and test motor coupled to the servo drive. The servo drive is utilized to maintain constant speed during torque measurement. The torque transducer is capable of measuring torque signal of up to 20Nm. The analog torque measurement data is captured for every encoder pulse. The encoder has 4096 pulses per revolution providing a measurement resolution of 0.088deg. The torque ripple measurements are made with the servo speed maintained at 40RPM. For torque ripple measurement at high speeds, a different dyno is utilized where stator reaction force measurements are used to measure the torque ripple. The inverter is switched at 16 kHz frequency and the control logic is implemented in an automotive-grade microcontroller.

The analysis results presented in Sections II and III are verified experimentally. Firstly the analysis of the magnitude ratio between the *d* and *q-axis* current cancellation for a set of operating points is validated. The operating points are shown in Table 4. For these operating points, the torque ripple cancellation currents are obtained experimentally by adjusting the injected current until the measured torque ripple is near zero, for both the *d* and *q-axis* based current cancellation. Since the 60th order torque ripple magnitude is the major component, the cancellation current magnitudes obtained for 60th order cancellation are summarized in Table 4. Fig. 12 compares the analytically obtained magnitude ratio with the experimental ratio for 60th order ripple cancellation. The difference between the analysis and the experimental result can be explained due

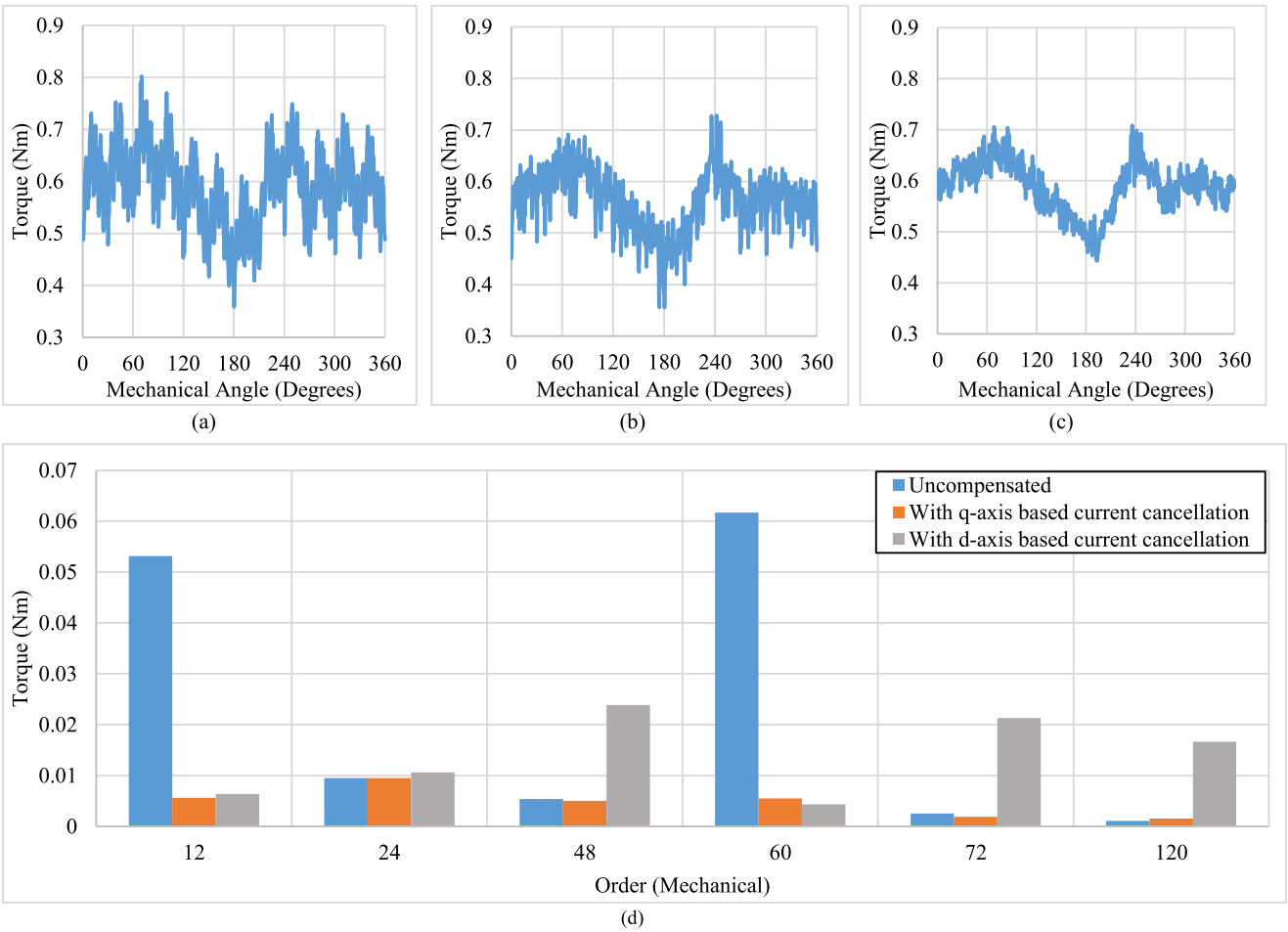

FIGURE 13. Experimental torque ripple results for Op.1 ($I_q = 12.5A$ and $I_d = 112.5A$). (a) Uncompensated torque ripple of the machine. (b) Compensated torque ripple after *d-axis* current based cancellation with $I_{dr,n_1} = 15.2A$ and $I_{dr,n_2} = 17.5A$. (c) Compensated torque ripple after *q-axis* current based cancellation with $I_{qr,n_1} = 1.7A$ and $I_{qr,n_2} = 1.9A$. (d) Harmonic component comparison between the uncompensated and compensated torque ripple after *q-axis* and *d-axis* current based cancellation.

to the difference between analytical parameters and the actual machine.

Secondly, Figs. 13 and 14 show the torque ripple orders before and after compensation for Op.1 and Op.2. For Op.1, the compensation current is applied in the *d-axis* and then in the *q-axis*. The intended 12^{th} and 60^{th} torque ripple orders are reduced with both *d* and *q-axis* current based cancellation. The cancellation current magnitudes required for I_d current based compensation are 15.2A for 12^{th} order and 17.5A for 60^{th} order torque ripple. While with the I_q current based compensation, the cancellation current magnitudes are 1.7A and 1.9A for 12^{th} and 60^{th} order torque ripple respectively. Also, as a consequence of the saturation, undesired orders (24^{th}, 48^{th}, $72^{nd,}$ and 120^{th}) of torque ripple are developed with I_d current based cancellation. No significant undesired torque ripple orders are created with I_q current based cancellation.

For Op.2, with I_q current based cancellation, the cancellation current magnitudes are 9.5A for 12^{th} order cancellation and 15.65A for 60^{th} order cancellation. The cancellation current magnitudes with I_d current based method are 0.6A for 12^{th} order cancellation and 1.11A for 60^{th} order cancellation. As a consequence of the saturation effect, with I_q current based cancellation undesired orders (24^{th}, 48^{th}, $72^{nd,}$ and 120^{th}) of torque ripple are created.

For Op.1 and Op.2, the experimental results of the compensated torque ripple orders follow the simulation results for the undesired torque ripple orders and the magnitude ratio of the compensating currents. Between the simulation and the experimental results the difference in the dc value of the torque can be explained by the parameter differences between the simulated and the actual machine. The difference in the magnitudes of the ripple current between the simulation and the experiment used for cancellation can also be explained by the difference in the assumed parameters vs the actual parameters of the machine. The lower orders observed in the experimental torque ripple graph are developed due to mechanical issues in the experimental setup.

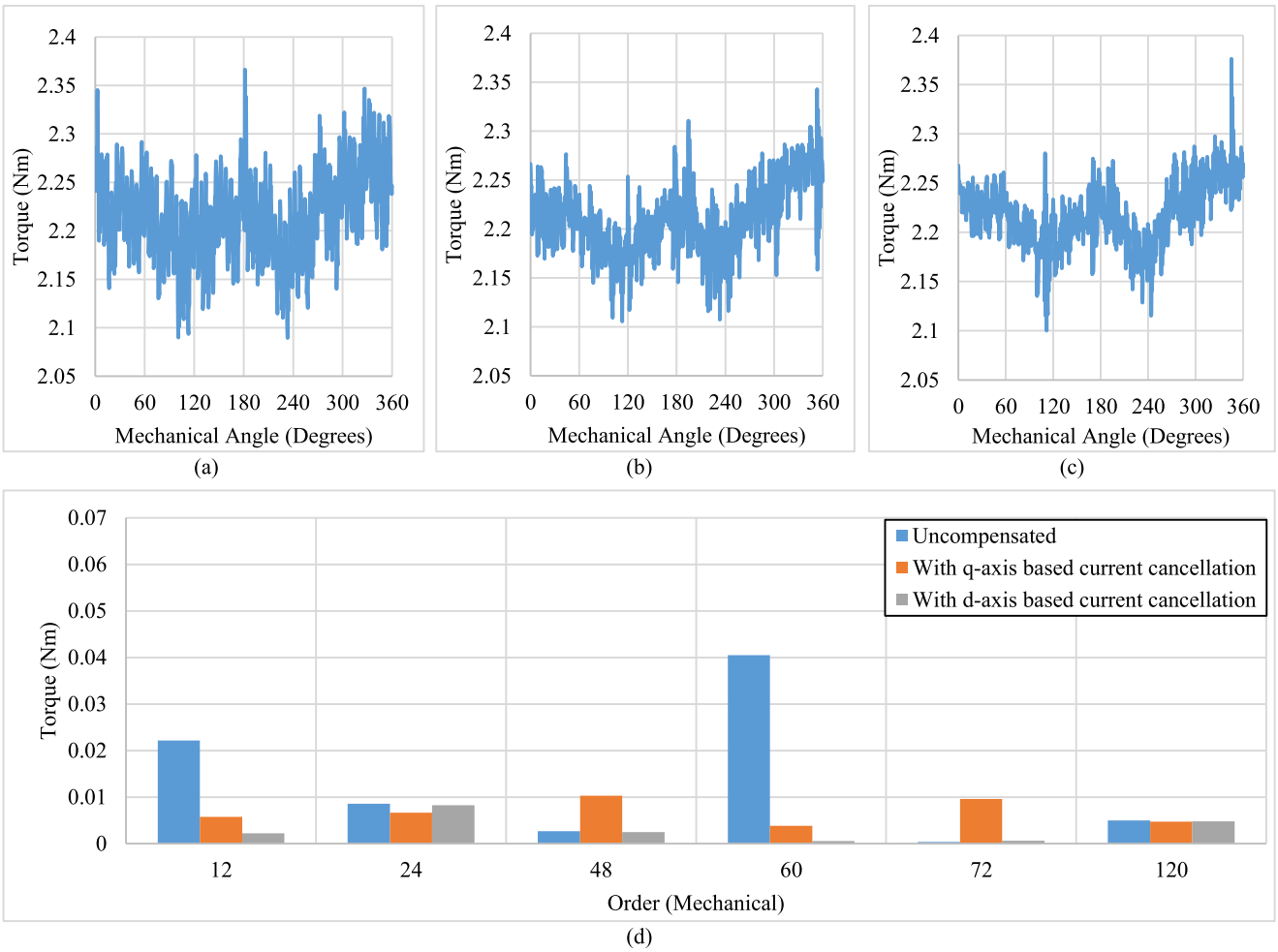

FIGURE 14. Experimental torque ripple results for Op.2 (I_q= 112.5A and I_d = 62.5A). (a) Uncompensated torque ripple of the machine. (b) Compensated torque ripple after q-axis current based cancellation (left) with $I_{qr,n_1} = 9.5A$ and $I_{qr,n_2} = 15.65A$. (c) Compensated torque ripple after d-axis current based cancellation (left) with $I_{dr,n_1} = 0.6A$ and $I_{dr,n_2} = 1.11A$. (d) Harmonic component comparison between the uncompensated and compensated torque ripple after q-axis and d-axis current based cancellation.

VI. CONCLUSION

The effectiveness of the *d* and *q-axis* current injection method for active torque ripple cancellation in SyRM is evaluated in this paper. The analysis is provided to determine which of the two methods is ideal for a given operating point (given I_d and I_q). It is also shown that the saturation can create undesired torque ripple components in addition to the desired compensating torque component. The magnitudes of the ripple current required for compensation in the *d* and the *q-axis* may differ by an order of magnitude at some operating points. It is also shown that an additional dc component may be produced due to saturation. The analysis is verified by experimental results.

REFERENCES

[1] A. Vagati, A. Canova, M. Chiampi, M. Pastorelli, and M. Repetto, "Design refinement of synchronous reluctance motors through finite-element analysis," *IEEE Trans. Ind. Appl.*, vol. 36, no. 4, pp. 1094–1102, Jul./Aug. 2000, doi: 10.1109/28.855965.

[2] W. Zhao, F. Xing, X. Wang, T. A. Lipo, and B. Kwon, "Design and analysis of a novel PM-assisted synchronous reluctance machine with axially integrated magnets by the finite-element method," *IEEE Trans. Magn.*, vol. 53, no. 6, Jun. 2017, Art no. 8104104, doi: 10.1109/TMAG.2017.2662717.

[3] C. Babetto, G. Bacco, and N. Bianchi, "Synchronous reluctance machine optimization for high-speed applications," *IEEE Trans. Energy Convers.*, vol. 33, no. 3, pp. 1266–1273, Sep. 2018, doi: 10.1109/TEC.2018.2800536.

[4] M. Sanada, K. Hiramoto, S. Morimoto, and Y. Takeda, "Torque ripple improvement for synchronous reluctance motor using an asymmetric flux barrier arrangement," *IEEE Trans. Ind. Appl.*, vol. 40, no. 4, pp. 1076–1082, Jul./Aug. 2004, doi: 10.1109/TIA.2004.830745.

[5] J. Tsuchiya, K. Mishima, and G. Kimura, "A study on torque ripple reduction of synchronous reluctance motor," in *Proc. 4th IEEE Int. Conf. Power Electron. Drive Syst.* , 2001, vol. 2, pp. 452–455, doi: 10.1109/PEDS.2001.975358.

[6] D. Yan, C. Xia, L. Guo, H. Wang, and T. Shi, "Design and analysis for torque ripple reduction in synchronous reluctance machine," *IEEE Trans. Magn.*, vol. 54, no. 11, Nov. 2018, Art. no. 8203605, doi: 10.1109/TMAG.2018.2847735.

[7] M. Chowdhury, A. Tesfamicael, M. Islam, and I. Husain, "Design optimization of a synchronous reluctance machine for high-performance applications," *IEEE Trans. Ind. Appl.*, vol. 57, no. 5, pp. 4720–4732, Sep./Oct. 2021, doi: 10.1109/TIA.2021.3091416.

[8] C. Liu, K. Wang, S. Wang, Y. Wang, and J. Zhu, "Torque ripple reduction of synchronous reluctance machine by using asymmetrical barriers and hybrid magnetic core," *CES Trans. Elect. Machines Syst.*, vol. 5, no. 1, pp. 13–20, Mar. 2021, doi: 10.30941/CESTEMS.2021.00003.

[9] H. Wu, D. Depernet, V. Lanfranchi, K. E. K. Benkara, and M. A. H. Rasid, "A novel and simple torque ripple minimization method of synchronous reluctance machine based on torque function method," *IEEE Trans. Ind. Electron.*, vol. 68, no. 1, pp. 92–102, Jan. 2021, doi: 10.1109/TIE.2019.2962490.

[10] Y. Ren and Z. Q. Zhu, "Reduction of both harmonic current and torque ripple for dual three-phase permanent-magnet synchronous machine using modified switching-table-based direct torque control," *IEEE Trans. Ind. Electron.*, vol. 62, no. 11, pp. 6671–6683, Nov. 2015, doi: 10.1109/TIE.2015.2448511.

[11] M. Saur, D. E. Gaona Erazo, J. Zdravkovic, B. Lehner, D. Gerling, and R. D. Lorenz, "Minimizing torque ripple of highly saturated salient pole synchronous machines by applying DB-DTFC," *IEEE Trans. Ind. Appl.*, vol. 53, no. 4, pp. 3643–3651, Jul./Aug. 2017, doi: 10.1109/TIA.2017.2684086.

[12] T. M. Jahns and W. L. Soong, "Pulsating torque minimization techniques for permanent magnet AC motor drives-a review," *IEEE Trans. Ind. Electron.*, vol. 43, no. 2, pp. 321–330, Apr. 1996, doi: 10.1109/41.491356.

[13] Luocheng Yan, Yong Liao, Hao Lin, and Jun Sun, "Torque ripple suppression of permanent magnet synchronous machines by minimal harmonic current injection," *IET Power Electron.*, vol. 12, no. 6, pp. 1368–1375, 2019, doi: 10.1049/iet-pel.2018.5647.

[14] P. Mattavelli, L. Tubiana, and M. Zigliotto, "Torque-ripple reduction in PM synchronous motor drives using repetitive current control," *IEEE Trans. Power Electron.*, vol. 20, no. 6, pp. 1423–1431, Nov. 2005, doi: 10.1109/TPEL.2005.857559.

[15] C. Lai, G. Feng, K. Mukherjee, V. Loukanov, and N. C. Kar, "Torque ripple minimization for interior PMSM with consideration of magnetic saturation incorporating online parameter identification," *IEEE Trans. Magn.*, vol. 53, no. 6, Jun. 2017, Art no. 8105904, doi: 10.1109/TMAG.2017.2666089.

[16] L. Springob and J. Holtz, "High-bandwidth current control for torque-ripple compensation in PM synchronous machines," *IEEE Trans. Ind. Electron.*, vol. 45, no. 5, pp. 713–721, Oct. 1998, doi: 10.1109/41.720327.

[17] N. Nakao and K. Akatsu, "Suppressing pulsating torques: Torque ripple control for synchronous motors," *IEEE Ind. Appl. Mag.*, vol. 20, no. 6, pp. 33–44, Nov./Dec. 2014, doi: 10.1109/MIAS.2013.2288383.

[18] P. L. Chapman, S. D. Sudhoff, and C. A. Whitcomb, "Optimal current control strategies for surface-mounted permanent-magnet synchronous machine drives," *IEEE Trans. Energy Convers.*, vol. 14, no. 4, pp. 1043–1050, Dec. 1999, doi: 10.1109/60.815026.

[19] J. Y. Hung and Z. Ding, "Minimization of torque ripple in permanent magnet motors: A closed form solution," in *Proc. Int. Conf. Ind. Electron., Control, Instrum., Automat.*, vol. 1, 1992, pp. 459–463, doi: 10.1109/IECON.1992.254563.

[20] R. Carlson, A. A. Tavares, J. P. Bastos, and M. Lajoie-Mazenc, "Torque ripple attenuation in permanent magnet synchronous motors," in *Proc. Conf. Rec. IEEE Ind. Appl. Soc. Annu. Meeting*, 1989, vol. 1, pp. 57–62, doi: 10.1109/IAS.1989.96631.

[21] B. Nogarede and M. Lajoie-Mazenc, "Torque ripple minimisation methods in sinusoidal fed synchronous permanent magnet machines," in *Proc. 5th Int. Conf. Elect. Machines Drives*, 1991, pp. 41–45.

[22] C. Jia, T. Sun, G. Yu, D. Lin, and J. Liang, "Torque ripple minimization of IPMSM drives with current injection derived from torque error," in *Proc. 8th Int. Conf. Power Electron. Syst. Appl.*, 2020, pp. 1–6, doi: 10.1109/PESA50370.2020.9344030.

[23] A. Houari, F. Auger, J. Olivier, and M. Machmoum, "A new compensation technique for PMSM torque ripple minimization," in *Proc. IEEE Ind. Appl. Soc. Annu. Meeting*, 2015, pp. 1–6, doi: 10.1109/IAS.2015.7356827.

[24] I. Kärkkäinen and A. Arkkio, "Harmonic torque suppression by manual voltage injection," in *Proc. XIX Int. Conf. Elect. Machines*, 2010, pp. 1–6, doi: 10.1109/ICELMACH.2010.5608064.

[25] H. Kim and S. Bhattacharya, "A novel current control strategy based on harmonic voltage injection for power losses reduction of PMSMs with non-sinusoidal Back-EMF," in *Proc. IEEE Ind. Appl. Soc. Annu. Meeting*, 2019, pp. 1–6, doi: 10.1109/IAS.2019.8912372.

[26] A. K. Singh, R. Raja, T. Sebastian, A. Shrestha, M. Sariful Islam, and K. Rajashekara, "A novel control strategy to mitigate the parameter saturation problems in synchronous reluctance machines," in *Proc. IECON–47th Annu. Conf. IEEE Ind. Electron. Soc* ., 2021, pp. 1–6, doi: 10.1109/IECON48115.2021.9589407.

[27] A. Gebregergis *et al.*, "Motor control system to compensate for toroue ripple," U.S. Patent 9,136,785 B2, 2015.

[28] A. K. Singh, R. Raja, T. Sebastian, and K. Rajashekara, "Torque ripple minimization control strategy in synchronous reluctance machines," in *Proc. 47th Annu. Conf. IEEE Ind. Electron. Soc.*, 2021, pp. 1–6, doi: 10.1109/IECON48115.2021.9589827.

[29] A. K. Singh, R. Raja, T. Sebastian, and A. Ali, "Limitations of the PI control with respect to parameter variation in PMSM motor drive systems," in *Proc. IEEE Int. Electric Machines Drives Conf.*, 2019, pp. 1688–1693, doi: 10.1109/IEMDC.2019.8785406.